High contribution of anthropogenic combustion sources to atmospheric inorganic reactive nitrogen in South China evidenced by isotopes

Tingting Li[1,2,4], Jun Li[*1,2], Zeyu Sun[3,4], Hongxing Jiang[1], Chongguo Tian[3], Gan Zhang[1,2]

[1]State Key Laboratory of Organic Geochemistry and Guangdong province Key Laboratory of Environmental Protection and Resources Utilization, Guangdong-Hong Kong-Macao Joint Laboratory for Environmental Pollution and Control, Guangzhou Institute of Geochemistry, Chinese Academy of Sciences, Guangzhou, 510640, China

[2]CAS Center for Excellence in Deep Earth Science, Guangzhou 510640, P. R. China

[3]Yantai Institute of Coastal Zone Research, Chinese Academy of Sciences, Yantai 264003, P. R. China

[4]University of Chinese Academy of Sciences, Beijing 100049, P. R. China

**Correspondence to*: Jun Li (junli@gig.ac.cn)

Abstract: Due to the intense release of reactive nitrogen (Nr) from anthropogenic activity, the source layout of atmospheric nitrogen aerosol has changed. The inorganic nitrogen (NH_4^+ and NO_3^-) was essential part of atmospheric nitrogen aerosol and accounted for 69%. To comprehensively clarify the level, sources, and environmental fate of NH_4^+ and NO_3^-, their concentrations and stable isotopes ($\delta^{15}N$) in fine particulate matters ($PM_{2.5}$) were measured in a subtropical megacity of South China. N-NH_4^+ and N-NO_3^- contributed 45.8% and 23.2% to total nitrogen (TN), respectively. The source contributions of NH_4^+ and NO_3^- were estimated by $\delta^{15}N$, which suggested that anthropogenic combustion activities including coal combustion, biomass burning, and vehicles were dominant sources. Especially, biomass burning was the predominant source of NH_4^+ (27.9%). Whereas, coal combustion was the dominant source of NO_3^- (40.4%). This study emphasized the substantial impacts of human activities on inorganic Nr. With the rapid development of industry and transportation, nitrogen emissions will be even higher. The promotion of clean energy and efficient use of biomass would help reduce nitrogen emissions and alleviate air pollution.

1. Introduction

Nitrogenous aerosols are ubiquitous in environment and play an important role as nutrients in ecosystems(Bhattarai et al., 2019). With the massive combustion of fossil fuels and the development of livestock, the proportion of TN in particulate matter (PM) ranges from 1.2% to 17.0% and has shown a rapid increase in the last few decades(Bhattarai et al., 2019; Galloway et al., 2004; Holland et al., 1999). Mostly nitrogenous aerosols formed from atmospheric Nr will be deposited into terrestrial and aquatic ecosystems(Huang et al., 2015). Excessive external nitrogen deposition accelerates nitrogen loss in soil, decreases species diversity, disturbs terrestrial ecosystems, and leads to eutrophication in aquatic ecosystems(Breemen, 2002; Wedin and Tilman, 1996; Yang et al., 2015). Furthermore, nitrogenous aerosols have adverse impacts on the climate, air quality, and human health(Bhattarai et al., 2019; Song et al., 2021).

$N\text{-}NO_3^-$ and $N\text{-}NH_4^+$ as inorganic Nr are dominant species in the deposition of nitrogen(Zhu et al., 2015). $N\text{-}NH_4^+$ was the highest in nitrogen deposition, and NH_4^+ was gradually considered to be an important component of secondary inorganic aerosols (SIA)(Sun et al., 2021). NH_3, the precursor of NH_4^+, is a vital atmospheric alkaline gas, which can participate in nucleation to promote new particles generation, and can react with acid gas to produce ammonium sulfate and ammonium nitrate(Dunne et al., 2016; Fu et al., 2017). The excessive NH_3 emission from anthropogenic sources will partially offset the benefits of reducing SO_2 and NOx and trigger urban haze in China(Sun et al., 2021; Meng et al., 2018; Pan et al., 2018a). In many urban environments, NO_3^- has replaced sulfate as the component with the highest proportion in SIA. NOx, precursors of NO_3^-, are also closely related to the formation of atmospheric oxidants and exert important effects on atmospheric oxidation. In addition, NH_4NO_3 in PM plays an increasingly important role in promoting the formation of sulfate and organic matter, and has profound effect on the physical and chemical properties of PM(Liu et al., 2021; Liu et al., 2020; Hodas et al., 2014). Therefore, to mitigate nitrogen deposition and air pollution, the control of NH_4^+ (NH_3) and NO_3^- (NOx) should not be neglected.

Considerable efforts have been made to comprehensively understand the budget of atmospheric NH_4^+ and NO_3^-. $\delta^{15}N$ is effective to quantify sources contribution of nitrogenous

59 species(Elliott et al., 2007). The anthropogenic combustion sources (combustion of coal,
60 biomass, and gasoline) play a key role in the emission of NO_3^- (NOx) in many regions of China
61 suggested by $\delta^{15}N$(Zong et al., 2020), which also have large effects on NH_3(Chen et al., 2022b).
62 NH_3 is released by agricultural sources (agricultural activity and livestock) and non-agricultural
63 sources (fossil fuel combustion and vehicle)(Bhattarai et al., 2019). A previous study showed
64 that agricultural source was the dominant source (80%-90%) of NH_3 in China(Kang et al.,
65 2016). However, NH_3 emissions from agricultural source have been reduced due to intensive
66 farming and efficient fertilization(Wang et al., 2022). The incomplete burning of biomass leads
67 to massive NH_3 emissions and is gradually to be the second largest non-agricultural source of
68 NH_3(Yu et al., 2020), which may be responsible for the lag of the decline in air pollutants
69 deposition behind the reduction in emission of precursors(Zhao et al., 2022b). Biomass burning
70 in the suburbs also has a potential impact on urban NH_3(Xiao et al., 2020). As for urban NH_3,
71 combustion sources (including coal combustion, vehicles emission, and biomass burning) were
72 gradually becoming dominant sources in recent years verified by $\delta^{15}N$-NHx (NH_3+NH_4^+)(Xiao
73 et al., 2020; Pan et al., 2018b). In addition, the super clean emission of coal-fired power plant
74 and strict emission standards of vehicles will change the source layout of NH_4^+ and NO_3^-.
75 Selective catalytic reduction technology equipped with vehicles and industrial boiler reduces
76 NOx but increases NH_3 emissions(Meng et al., 2017; Pan et al., 2016). The occurrence of haze
77 in North China was closely related to NH_3 emissions from combustion sources(Pan et al., 2018a;
78 Pan et al., 2018b). NH_4^+ and NO_3^- are the main components of SIA and play a vital role in the
79 formation of secondary aerosol(Meng et al., 2017), so it is necessary to revisit their sources.
80 Nr emissions from densely populated subtropical areas increased rapidly with the high
81 development of industry and transportation(Wang et al., 2013). Guangzhou is the core megacity
82 in the South subtropical region of China, where the atmospheric environment is complex and
83 the atmospheric oxidation level is high(Tan et al., 2019). The high emissions of inorganic
84 nitrogen from anthropogenic combustion sources have serious and profound impacts on the
85 environment. In this study, we aimed to comprehensively clarify the level of inorganic Nr and
86 revisit the source layout of atmospheric inorganic Nr.

2. Experimental and theoretical methods

2.1. Sampling and Chemical concentration analysis

$PM_{2.5}$ samples (n=66) were collected from May 2017 to June 2018 in Guangzhou (23.13°N, 113.27°E). Details of sample collection can be found in our previous study(Jiang et al., 2021a). The chemical components including water-soluble ions (i.e., NH_4^+, K^+, Na^+, Ca^{2+}, Mg^{2+}, Cl^-, NO_3^-, and SO_4^{2-}), organic carbon (OC), element carbon (EC), and organic molecular markers (e.g., levoglucosan) were analyzed in our previous studies (**SI Text S1**)(Jiang et al., 2021a; Jiang et al., 2021b). Moreover, meteorological parameters (temperature, relative humidity (RH), atmosphere pressure, and wind speed) and the concentration of trace gases (CO, SO_2, NO, NO_2, and O_3) were acquired by online instruments (details shown in **SI Text S1**). A circular punch (r=1cm) of the sample filter was wrapped in a tin boat and then measured in an elemental analyzer to determine the concentrations of TN.

2.2. Isotope analysis

The $\delta^{15}N\text{-}NO_3^-$ and $\delta^{18}O\text{-}NO_3^-$ values in $PM_{2.5}$ were analyzed by methods of nitrous oxide (N_2O), which was described in previous study in detail(Zong et al., 2017). Briefly, NO_3^- was reduced to NO_2^- using cadmium powder and imidazole solution, and N_2O was made by adding NaN_3 to NO_2^- solution. The production of 75nmol N_2O gas was needed to measure. The N_2O gas produced by above processes was measured by MAT253 stable isotope mass spectrometer. The values of $\delta^{18}O$ and $\delta^{15}N$ were expressed in per mil (‰) shown in Eq. (1) and (2), relative to the international oxygen and nitrogen isotope standard, respectively.

$$\delta^{15}N = \left[\frac{(^{15}N/^{14}N)_{sample}}{(^{15}N/^{14}N)_{standard}} - 1\right] * 1000 \quad (1)$$

$$\delta^{18}O = \left[\frac{(^{18}O/^{16}O)_{sample}}{(^{18}O/^{16}O)_{standard}} - 1\right] * 1000 \quad (2)$$

The $\delta^{15}N\text{-}NH_4^+$ was measured by methods of hypobromite oxidation coupled with reduction of hydroxylamine hydrochloride(Sun et al., 2021). Briefly, NH_4^+ was oxidated to NO_2^- using alkaline hypobromite (BrO^-), and N_2O was made by adding sodium arsenite and hydrochloric acid to NO_2^- solution. The production of 120 nmol N_2O gas was needed to measure. The N_2O gas produced by above processes was measured by MAT253 stable isotope mass spectrometer. The values of $\delta^{15}N$ were expressed in per mil (‰), Eq. (1). To ensure the

stability of the instrument, standard samples were tested for every ten samples. The standard deviation of replicates was generally less than 0.4‰, 0.8‰, and 0.5‰ for $\delta^{15}N\text{-}NO_3^-$, $\delta^{18}O\text{-}NO_3^-$, and $\delta^{15}N\text{-}NH_4^+$, respectively. The instrumental values of $\delta^{15}N\text{-}NO_3^-$ and $\delta^{18}O\text{-}NO_3^-$ were corrected by multi-point correction ($\delta^{18}O$ r^2=0.99, $\delta^{15}N$ r^2=0.999) based on international standards (IAEA-NO-3, USGS32, USGS34, and USGS35). The measured values of $\delta^{15}N\text{-}NH_4^+$ were also corrected by multi-point correction (r^2=0.999) based on international standards (IAEA-N1, USGS25, and USGS26). In addition, ^7Be and ^{210}Pb were acquired and details were shown in **SI Text S1**.

2.3. IsoSource and Bayesian mixing model

IsoSource model. IsoSource model was released by Environmental Protection Agency (EPA), could calculate ranges of source contributions to a mixture based on conservation of isotopic mass when number of sources is too large to permit a unique solution and provide the distribution of source proportions (Phillips et al., 2005). IsoSource model coupled with $\delta^{15}N\text{-}NH_3$ of atmospheric initial and potential sources (shown in **Table 1**) were applied to quantify the contribution of various sources to NH_3. Nitrogen fertilizers application, livestock, human waste, biomass burning, coal combustion, and vehicles were considered as sources of NH_3 in this study, details shown in **SI Text S2**. Atmospheric initial $\delta^{15}N\text{-}NH_3$ was calculated by following Eq. (3).

$$\delta^{15}N\text{-}NH_{3\text{-initial}} = \delta^{15}N\text{-}NH_4^+ - \varepsilon(NH_4^+\text{-}NH_3) \times (1 - f) \quad (3)$$

Where, $\delta^{15}N\text{-}NH_4^+$ and $\delta^{15}N\text{-}NH_{3\text{-initial}}$ represent the $\delta^{15}N$ of particulate NH_4^+ and atmospheric initial NH_3, respectively. $\varepsilon(NH_4^+\text{-}NH_3)$ represents the isotope fractionation factor in the gaseous NH_3 conversion to particulate NH_4^+ in the atmosphere. The f value represents the proportion of the initial NH_3 converted to NH_4^+, referring to NH_3 and NH_4^+ observed in Guangzhou (Liao et al., 2014).

The $\varepsilon(NH_4^+\text{-}NH_3)$ value is temperature dependent(Huang et al., 2019), which can be deduced from(Urey, 1947), as shown in Eq. (4). The atmospheric average temperature was 24.5℃ in our sampling period, and the corresponding $\varepsilon(NH_4^+\text{-}NH_3)$ value was 34.2‰ calculated by Eq. (4). In addition, the $\varepsilon(NH_4^+\text{-}NH_3)$ in Guangzhou was estimated to be 32.4‰ according to Eq. (8). Eq. (8) was deduced by Eq. (5-7). According to Eq. (8), a linear fitting

144 equation was observed between fNH_4^+ and $\delta^{15}N\text{-}NH_4^+$ (**Fig. S1**), and the absolute value of the
145 slope (32.4‰) was equal to $\varepsilon(NH_4^+\text{-}NH_3)$. The $\varepsilon(NH_4^+\text{-}NH_3)$ average of the two methods (34.2‰
146 and 32.4‰) was 33.3‰ and approximated to the experimental isotope enrichment factor
147 (33‰)(Heaton et al., 1997). Therefore, 33‰ was used for deducing the $\delta^{15}N$ of the initial NH_3.

148 $$\varepsilon_{(NH_4^+\_NH_3)} = 12.4678 * \frac{1000}{T+273.15} - 7.6694 \quad (4)$$

149 $$\delta^{15}N\text{-}NH_4^+ - \delta^{15}N\text{-}NH_3 = \varepsilon_{(NH_4^+\_NH_3)} \quad (5)$$

150 $$fNH_4^+ + fNH_3 = 1 \quad (6)$$

151 $$\delta^{15}N\text{-}NH_4^+ * fNH_4^+ + \left(\delta^{15}N\text{-}NH_4^+ - \varepsilon_{(NH_4^+\_NH_3)}\right) * (1 - fNH_4^+) = \delta^{15}N \quad (7)$$

152 $$\delta^{15}N\text{-}NH_4^+ = -\varepsilon_{(NH_4^+\_NH_3)} * fNH_4^+ + (\delta^{15}N + \varepsilon_{(NH_4^+\_NH_3)}) \quad (8)$$

153 Where, T represents the atmospheric temperature (°C). $\delta^{15}N\text{-}NH_4^+$ and $\delta^{15}N\text{-}NH_3$
154 represent the $\delta^{15}N$ of particulate NH_4^+ and atmospheric NH_3, respectively. $\delta^{15}N$ represents the
155 sum of $\delta^{15}N\text{-}NH_4^+$ and $\delta^{15}N\text{-}NH_3$. fNH_3 and fNH_4^+ represent the proportion of atmospheric
156 NH_3 and particulate NH_4^+, respectively.

157 **Bayesian mixing model.** $\delta^{15}N$ were used for tracing source based on conservation of
158 isotopic mass. Bayesian mixing model improved upon linear mixing models by explicitly
159 considering uncertainty in prior information and isotopic equilibrium fractionation. Recently,
160 Bayesian mixing model was applied to trace the sources of atmospheric pollutants(Zong et al.,
161 2017; Zong et al., 2020). The model coupled with $\delta^{15}N\text{-}NO_3^-$ and $\delta^{18}O\text{-}NO_3^-$ were used to
162 identify the formation process and quantify the sources contribution of NO_3^-.

163 In Central Pearl River Delta (PRD), NO_3^- formed through ·OH and N_2O_5 pathways
164 contributed to 94% simulated by CAMQ model (Qu et al., 2021). In this study, only ·OH and
165 N_2O_5 formation pathways were considered. Details of NO_3^- formation pathway were also
166 shown in **SI Text S2**. The atmospheric $\delta^{18}O\text{-}NO_3^-$ can be expressed by Eq. (9). The $[\delta^{18}O\text{-}HNO_3]_{OH}$
167 can be further expressed by Eq. (10) assuming no kinetic isotope fractionation
168 (Walters and Michalski, 2016). And $[\delta^{18}O\text{-}HNO_3]_{H2O}$ can be estimated by Eq. (11) (Walters and
169 Michalski, 2016). The $\delta^{18}O$ values in tropospheric H_2O, NOx, O_3, and OH were within a certain
170 range. The tropospheric $\delta^{18}O\text{-}H_2O$, $\delta^{18}O\text{-}NOx$, $\delta^{18}O\text{-}O_3$, and $\delta^{18}O\text{-}OH$ ranged from -25‰ to
171 0‰(Baskaran et al., 2011; Walters and Michalski, 2016), 112‰ to 122‰ (Michalski et al.,

2014; Walters and Michalski, 2016), 90‰ to 122‰, and -15‰ to 0‰, respectively(Fang et al., 2011; Johnston and Thiemens, 1997). Therefore, the γ (the contribution of ·OH formation pathway) can be estimated by $f$$NO_2$ and oxygen isotope fractionation i.e., αNO_2/NO, αOH/H_2O, and αN_2O_5/NO_2. The oxygen isotope fractionations are temperature dependent and can be estimated by Eq. (13) and **Table S1.** The $f$$NO_2$ varied from 0.20 to 0.95(Zong et al., 2017; Walters et al., 2016). Based on $\delta^{18}O$-NO_3^-, $\delta^{18}O$-H_2O, $\delta^{18}O$-NOx, $\delta^{18}O$-O_3, and temperature (Eq. (9-13)), γ (maximum γ and minimum γ) was estimated by Monte Carlo simulation nested in Bayesian mixing model (Zong et al., 2017). Assuming no kinetic isotope fractionation, the nitrogen isotope fractionation value in the formation process of NO_3^- (εN) was calculated by Eq. (13-16) combined with γ and temperature (Zong et al., 2017; Walters and Michalski, 2016; Walters et al., 2016). The εN value in our sampling period was 5.1±2.5‰, which was comparable to that in Beijing(average 6.5‰)(Fan et al., 2020). The contributions of different sources to atmospheric NOx were quantified by Bayesian mixing model coupled with εN, $\delta^{15}N$-atmospheric-NO_3^-, and $\delta^{15}N$-NOx endmembers shown in **Table 1**. We considered coal combustion, mobile traffic sources, biomass burning, and soil microbial process as dominant atmospheric NOx sources in Guangzhou, details shown in **SI Text S2**. The specific details of Bayesian mixing model were reported by our previous studies(Zong et al., 2017; Zong et al., 2020).

$$\delta^{18}O\text{-}NO_3^- = \gamma \times [\delta^{18}O\text{-}NO_3^-]_{OH} + (1-\gamma) \times [\delta^{18}O\text{-}NO_3^-]_{H_2O} = \gamma \times [\delta^{18}O\text{-}HNO_3]_{OH} + (1-\gamma) \times [\delta^{18}O\text{-}HNO_3]_{H_2O} \quad (9)$$

$$[\delta^{18}O\text{-}HNO_3]_{OH} = \frac{2}{3}[(\delta^{18}O\text{-}NO_2)]_{OH} + \frac{1}{3}[\delta^{18}O\text{-}OH]_{OH} = \frac{2}{3}\left[\frac{1000\times(^{18}\alpha_{NO_2/NO}-1)(1-f_{NO_2})}{(1-f_{NO_2})+(^{18}\alpha_{NO_2/NO}\times f_{NO_2})} + [\delta^{18}O\text{-}NO_X]\right] + \frac{1}{3}[(\delta^{18}O\text{-}H_2O) + 1000 \times (^{18}\alpha_{OH/H_2O} - 1)] \quad (10)$$

$$[\delta^{18}O\text{-}HNO_3]_{H_2O} = \frac{5}{6}(\delta^{18}O\text{-}N_2O_5) + \frac{1}{6}(\delta^{18}O\text{-}H_2O) \quad (11)$$

$$\delta^{18}O\text{-}N_2O_5 = \delta^{18}O\text{-}NO_2 + 1000 \times \left(^{18}\alpha_{N_2O_5/NO_2} - 1\right) \quad (12)$$

$$1000(^{m}\alpha_{X/Y} - 1) = \frac{A}{T^4} \times 10^{10} + \frac{B}{T^3} \times 10^{8} + \frac{C}{T^2} \times 10^{6} + \frac{D}{T} \times 10^{4} \quad (13)$$

$$\varepsilon N = \gamma \times \varepsilon(\delta^{15}N\text{-}NO_3^-)_{OH} + (1-\gamma) \times \varepsilon(\delta^{15}N\text{-}NO_3^-)_{H_2O}$$

$$= \gamma \times \varepsilon(\delta^{15}\text{N-}HNO_3)_{OH} + (1-\gamma) \times \varepsilon(\delta^{15}\text{N-}HNO_3)_{H_2O} \quad (14)$$

$$\varepsilon(\delta^{15}\text{N-}HNO_3)_{OH} = \varepsilon(\delta^{15}\text{N-}NO_2)_{OH} = 1000 \times \left[\frac{(^{15}\alpha_{NO_2/NO}-1)(1-f_{NO_2})}{(1-f_{NO_2})+(^{15}\alpha_{NO_2/NO}\times f_{NO_2})}\right] \quad (15)$$

$$\varepsilon(\delta^{15}\text{N-}HNO_3)_{H_2O} = \varepsilon(\delta^{15}\text{N-}N_2O_5)_{H_2O} = 1000 \times \left(^{15}\alpha_{N_2O_5/NO_2} - 1\right) \quad (16)$$

Where, γ is the contribution of ·OH formation pathway to NO_3^-, εN is the nitrogen isotope fractionation value. *f*NO_2 is the fraction of NO_2 in the total NOx. $^{18}\alpha NO_2/NO$, $^{18}\alpha OH/H_2O$, $^{18}\alpha N_2O_5/NO_2$ are the oxygen isotope equilibrium fractionation factors between NO_2 and NO, ·OH and H_2O, N_2O_5 and NO_2, respectively. $^{15}\alpha NO_2/NO$ and $^{15}\alpha N_2O_5/NO_2$ are the nitrogen isotope equilibrium fractionation factor between NO_2 and NO, N_2O_5 and NO_2, respectively.

Table 1. The estimation of δ^{15}N-NH_3 and δ^{15}N-NOx from various sources.

Source	δ^{15}N-NH_3(‰)	References
Biomass burning	17.5±7.8	(Kawashima and Kurahashi, 2011; Xiao et al., 2020)
Coal combustion	-2.5±6.4	(Felix et al., 2013; Pan et al., 2016)
Urban traffic	6.6±2.1	(Walters et al., 2020)
Fertilizer	-28.3±5.8	(Bhattarai et al., 2021; Chang et al., 2016; Felix et al., 2013; Bhattarai et al., 2020)
Livestock	-18.3±7.7	(Bhattarai et al., 2021; Chang et al., 2016; Felix et al., 2013; Bhattarai et al., 2020)
Urban waste	-22.8±3.6	(Bhattarai et al., 2021; Chang et al., 2016)
Source	δ^{15}N-NOx(‰)	References
Biomass burning	1.04±4.13	(Zong et al., 2017; Fibiger and Hastings, 2016; Zong et al., 2022)
Coal combustion	13.72±4.57	(Zong et al., 2017; Felix et al., 2015; Felix et al., 2012)
Mobile source	-7.25±7.80	(Zong et al., 2017; Walters et al., 2015)
Soil microbial process	-33.77±12.16	(Zong et al., 2017; Felix and Elliott, 2013)

3. Results and discussion

3.1. Concentration and seasonal variation of NH_4^+ and NO_3^-

The concentration of NH_4^+ and NO_3^- in $PM_{2.5}$ was 1.6±1.3 μg m^{-3} and 2.8±3.4 μg m^{-3}, contributed 18.7% and 32.6% to SIA. The concentration of N-NH_4^+ and N-NO_3^- was 1.2±1.0 μg m^{-3} and 0.6±0.8 μg m^{-3}, contributed 45.8% and 23.2% to TN, respectively; thus, NH_4^+ and NO_3^- were essential part of nitrogen aerosols. NH_4^+ and NO_3^- showed similar seasonal variations with higher concentrations in winter than in summer (**Fig. 1**). During winter the air mass was often dry and cold with low wind speed, which meant the decrease of the atmospheric self-purification capability. In addition, primary combustion sources related to fossil fuel and biomass burning always showed significant increase in North China in winter, which greatly

increased the concentration of atmospheric pollutants in Guangzhou by long-range transportation. However, during summer, the air mass from sea was relatively clean with high wind speed facilitating the diffusion of pollutants. Moreover, high temperature in summer was conducive to the decomposition of NH_4NO_3(Song et al., 2008). Thus, the levels of NH_4^+ and NO_3^- were lower in summer. In addition, concentrations of NH_4^+ and NO_3^- in our study, were lower than North China [Beijing(Wu et al., 2019; Fan et al., 2022), Tianjin(Xiang et al., 2022), Shijiazhuang(Xiang et al., 2022), and Harbin(Sun et al., 2021)], East China [Nanchang(Xiao et al., 2020)], and Central China [Wuhan and Changsha(Xiao et al., 2020; Zong et al., 2020)], suggested the level of air pollution in Guangzhou has been alleviated to a certain extent. Therefore, it is necessary to conduct comprehensive study on the emission sources of NH_4^+ and NO_3^- to take more effective measures to mitigate air pollution.

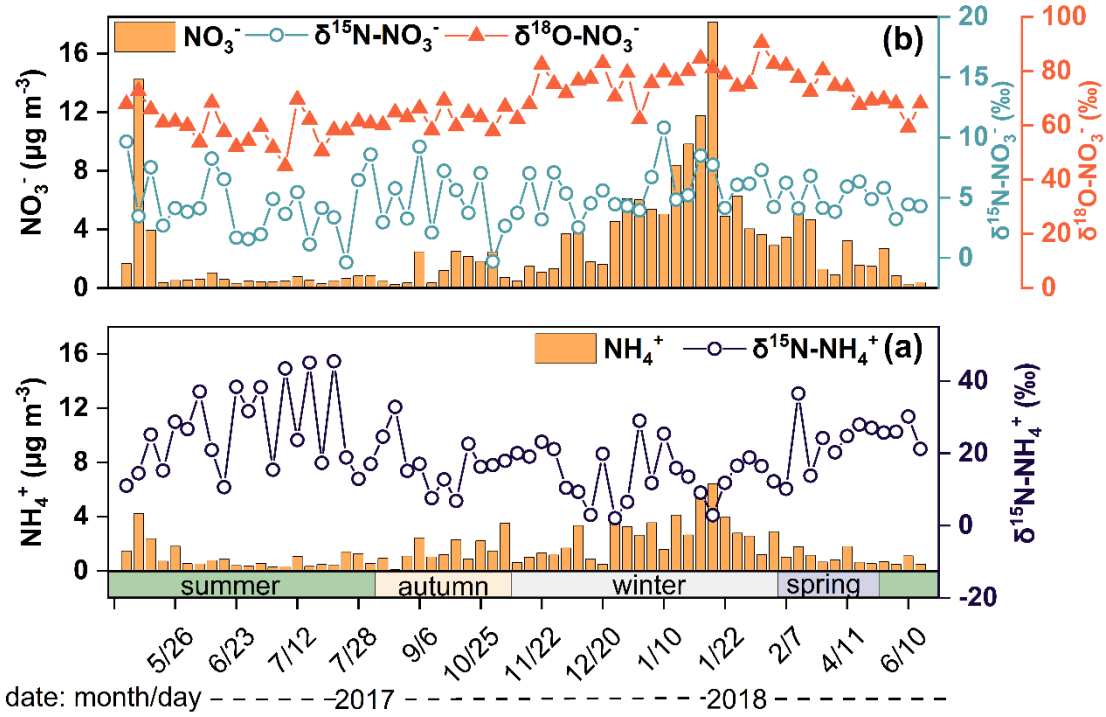

Figure 1. The concentration and $\delta^{15}N$ of NH_4^+ (a) and concentration, $\delta^{15}N$, and $\delta^{18}O$ of NO_3^- (b).

3.2. Characteristic and seasonal variation in $\delta^{15}N\text{-}NH_4^+$ and source apportionment of NH_4^+

The $\delta^{15}N\text{-}NH_4^+$ values over Guangzhou ranged from 2.1‰ to 45.5‰, with an annual mean of 20.2±10.1‰. In our study, the $\delta^{15}N\text{-}NH_4^+$ values were comparable to those at suburban sites (**Fig. S2**) such as sites in Japan (22.1±8.3‰, 16.1±6.6‰)(Kawashima and Kurahashi, 2011) and Korea (Jeju Island,17.4±4.9‰)(Kundu et al., 2010) but heavier than those in polluted regions, such as Guangzhou during summer haze(average 7.17‰)(Liu et al., 2018) and Beijing (-37.1‰ to 5.8‰)(Pan et al., 2016). $\delta^{15}N\text{-}NH_4^+$ values were lower in autumn (17.3‰) and winter (14.4‰) than in spring (22.5‰) and summer (25.7‰), which was similar to the trends in Japan(Kawashima and Kurahashi, 2011).

The seasonal differences in $\delta^{15}N\text{-}NH_4^+$ values were significant between warm (summer/spring) and cold seasons (winter/ autumn) ($p < 0.05$). The $\delta^{15}N\text{-}NH_4^+$ was affected by the ratio of $NH_4^+/(NH_3+NH_4^+)$ (Eq. (8) and **Fig. S1**). A linear fitting equation was observed between $NH_4^+/(NH_3+NH_4^+)$ and $\delta^{15}N\text{-}NH_4^+$, and the absolute value of the slope (32.4) approximated the isotope equilibrium fractionation value (33%) between atmospheric NH_3 and NH_4^+ (**Fig. S1**). The linear fitting suggested that the lower the NH_4^+ proportion was, the heavier the $\delta^{15}N\text{-}NH_4^+$ value. The lower NH_4^+ level was accordance with higher $\delta^{15}N\text{-}NH_4^+$ in summer, which was the opposite of winter. In addition, previous study suggested that the marked variation in $\delta^{15}N\text{-}NH_4^+$ values was largely controlled by the emission sources of NH_3, the precursor gas of NH_4^+(Liu et al., 2018). According to the $\delta^{15}N\text{-}NH_4^+$ results, the source of NH_4^+ was assigned as biomass burning (27.9±16.4%), coal combustion (16.0±3.9%), vehicles (19.8±5.3%), fertilizer (10.9±6.1%), livestock (12.7±5.8%), and urban waste (11.9±6.1%), shown in **Fig. 2a**.

In our study, non-agriculture sources were the dominators of NH_4^+ (75.6%). Unexpectedly, the contribution of biomass burning was the highest. Especially, from late June to July, the contribution of biomass burning enhanced, which possibly resulted from sugarcane leaf burning. The $\delta^{15}N$ in sugarcane leaf was as high as 38‰(Martinellia et al., 2002). The $\delta^{15}N$ of NH_4^+ formed from NH_3 released by sugarcane leaves burning was 44.1‰ (**SI Text S3**), which was consistent with the highest $\delta^{15}N\text{-}NH_4^+$ values (45.5‰ and 45.1‰) in July. In PRD, south winds prevail in July and the sampling site is located downwind of sugarcane planting area.

Therefore, the air mass to the sampling site might carry the pollutants related to sugarcane leaf burning. K^+ is a typical biomass burning tracer(Cui et al., 2018). Considering the impact of primary emission intensity, [NH_4^+/EC] and [K^+/EC] were used to calculate the correlation coefficient (r=0.435, $p < 0.01$), which verified NH_4^+ was influenced by biomass burning. In recent years, biomass burning has been gradually identified as an important source of NH_4^+(Meng et al., 2017; Xiao et al., 2020). The results based on emission inventories showed that the contribution of residential biomass combustion to NH_3 ranged from 33% to 53% in China(Meng et al., 2017). According to $\delta^{15}N$, biomass burning contributed 18% [Harbin, East North China](Sun et al., 2021), 46%[Wuhan, South Central China], 40% [Changsha, South Central China](Xiao et al., 2020), 35% [Nanchang, East China](Xiao et al., 2020), and 23% [Guangzhou, South China](Chen et al., 2022a) to NH_4^+. Particularly, in Guangzhou the contribution of biomass burning in the ground was higher than that in Guangzhou tower with a height of 488 meters, suggested that the influence of regional biomass burning(Chen et al., 2022a). Furthermore, ^7Be mainly originates from upper atmosphere, whereas ^{210}Pb is derived from terrestrial surface(Jiang et al., 2021b). High level of ^7Be observed in ground suggested the sink influence of upper atmosphere. ^7Be and ^{210}Pb are chemically stable and with unique sources, which can effectively reflect the transport of continental air mass and the air exchange between stratosphere and troposphere. In our study, the correlation coefficient between NH_4^+ and ^{210}Pb (r=0.701, $p < 0.01$) was higher than that between NH_4^+ and ^7Be (r=0.432, $p < 0.01$), suggested that NH_4^+ was mainly affected by regional emission. Therefore, biomass burning exerted essential influence on NH_4^+ level, which should no longer be ignored.

In addition, with the acceleration of urbanization, combustion sources related to fossil fuels have become the main sources of NH_3. In previous studies, the source of NH_x (NH_3+NH_4^+) was mainly from agricultural activity due to rough way of farming(Chang et al., 2016; Pan et al., 2020). However, with the improvement of efficient fertilization practices, agricultural NH_3 decreased significantly(Wang et al., 2022). Fossil fuels, such as coal and gasoline, are major energies for production and domestic using, and their contribution to NH_3 has become increasingly important. In North China, fossil fuel combustion contributed 92% to NH_3 during hazes(Zhang et al., 2020; Pan et al., 2016). In previous study of Guangzhou, the contribution of NH_3 from fossil source in ground observations (43%) was higher than the observed in

Guangzhou tower (18%), indicated the importance of locally related fossil fuel combustion source(Chen et al., 2022a). In our study, vehicle emission and coal combustion contributed 19.8±5.3% and 16.0±3.9% of NH_4^+ respectively, which was lower than North China but higher than agricultural sources. The share of NH_3 from vehicle exhaust was estimated to be 18.8% based on the emission factor of NH_3 from on road vehicles in Guangzhou, which was similar to our results(Liu et al., 2014). The selective catalytic reduction process for vehicle can reduce NOx, but increased emission of NH_3, which has confirmed as an important source of NH_3(Heeb et al., 2006; Meng et al., 2017). Despite the efforts of government to promote electric vehicles in recent years, their share is still relatively low (about 5%). As increasing car ownership, this has an important impact on atmospheric NH_3. Coal combustion was the second most important source of fossil combustion after vehicle emissions in our study, although the contribution was lower than in North China(Wu et al., 2019; Zhang et al., 2020; Pan et al., 2016). The absence of heating in Guangzhou may explain the lower contribution of coal combustion compared to the North. On an annual basis, the contribution of fossil fuel-related combustion sources in our study (35.8%) was comparable to that in North China (37%-52%)(Pan et al., 2018a).

The source contributions of NH_4^+ in our study were compared to other regions, shown in **Fig. S3**. The combustion related sources (biomass burning, coal combustion, and vehicle) have gradually become the dominant source of urban atmospheric NH_3. Biomass burning and vehicle could emit massive carbon monoxide (CO)(Li and Wang, 2007; Wang et al., 2005). In Guangzhou, NH_4^+ was positively related to CO (r=0.637, $p < 0.01$), which confirmed combustion sources played a key role in NH_4^+. From a historical perspective, NH_3 emissions from anthropogenic combustion and industry have been steadily increasing since 1960(Meng et al., 2017). The optimization of energy structure and encouragement of the development of new energy vehicle would be hopeful to reduce NH_3. The results of this study would be conducive to reducing NH_3 scientifically and effectively and would relieve the pressure on the reduction from agricultural source.

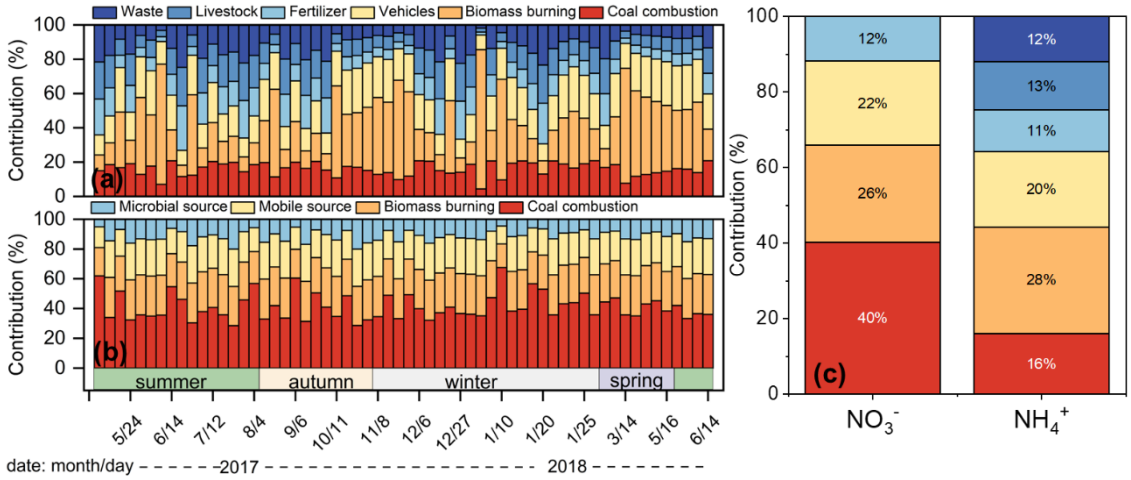

Figure 2. The sources apportionment results of atmospheric NH_4^+ (a) and NO_3^- (b) in Guangzhou, and the comparison of sources results between NH_4^+ and NO_3^- (c).

3.3. Characteristic and seasonal variation in $\delta^{18}O$-NO_3^- and $\delta^{15}N$-NO_3^- and source apportionment of NO_3^-

3.3.1. Seasonal variation of $\delta^{18}O$-NO_3^-

The $\delta^{18}O$-NO_3^- in Guangzhou was 68.1±9.7‰ (44.9‰ to 90.5‰) comparable to that in precipitation (66.3‰, ranging from 33.4‰ to 86.2‰)(Fang et al., 2011), but lower than those regions with weak light intensity, such as Beihuangcheng Island (ranging from 49.4‰ to 103.9‰)(Zong et al., 2017) and Bermuda Islands (cold season 76.9±6.3‰) (Hastings et al., 2003). In this study, $\delta^{18}O$-NO_3^- was higher in winter and spring than in summer and autumn, which was similar to the seasonal variation in $\delta^{18}O$-NO_3^- in previous studies (Fang et al., 2011; Gobel et al., 2013). On the one hand, $\delta^{18}O$-NO_3^- value was associated with the formation pathways of NO_3^-. The results simulated by Bayesian mixing model suggested that the contributions of N_2O_5 channel to NO_3^- were 56.8%, 58.9%, 29.2%, and 27.0% in winter, spring, autumn, and summer, respectively. The $\delta^{18}O$ value of NO_3^- formed by N_2O_5 channel is higher than that by ·OH pathway (**SI Text S2**). The night in cold season was longer than that in warm season, which favored NO_3^- formation through N_2O_5 channel. In addition, the illumination intensity was weakened in cold season compared with that in warm season, which constrained the production of ·OH(Zong et al., 2020; Tan et al., 2019; Wang et al., 2017). Thus, the contribution of the N_2O_5 channel in cold season was higher than that in warm season.

Furthermore, concentration of NO_3^- was high when contribution of N_2O_5 channel enhanced (**Fig. 3**), suggested NO_3^- pollution was related to N_2O_5 hydrolysis pathway. The air mass to Guangzhou was derived from the South China Sea in summer and the North continental region in winter. The higher $\delta^{18}O\text{-}NO_3^-$ and NO_3^- concentration might be affected by long-range and high-altitude transport from North China, which might carry abundant precursors. Massive NO_3^- could be formed by N_2O_5 hydrolysis at high altitude and transported to the ground. The index of $f(^7Be,^{210}Pb)$ was expressed in **SI Text S1** and could reflect the influence of atmospheric dynamic transport on aerosol pollutants(Jiang et al., 2021b). Generally, air masses with low values of $f(^7Be,^{210}Pb)$ suggested that pollutants were associated with continental surface emission, whereas high $f(^7Be,^{210}Pb)$ were influenced by long-range transport from upper air masses. The contribution of N_2O_5 channel was positively correlated with $f(^7Be,^{210}Pb)$ ($r=0.319$, $p < 0.05$), indicated the long-range transport influence of upper air mass on N_2O_5 channel. For example, on 25 January 2018, the contribution of N_2O_5 channel (nitrate) was 81.1% (3.6 μg m^{-3}), when the upper air mass was from North China. However, on 7 July 2017, the N_2O_5 channel (nitrate) contributed only 5.7% (0.5 μg m^{-3}) corresponding to the air mass mainly from the South China Sea transported at low-altitude (**Fig. S4**).

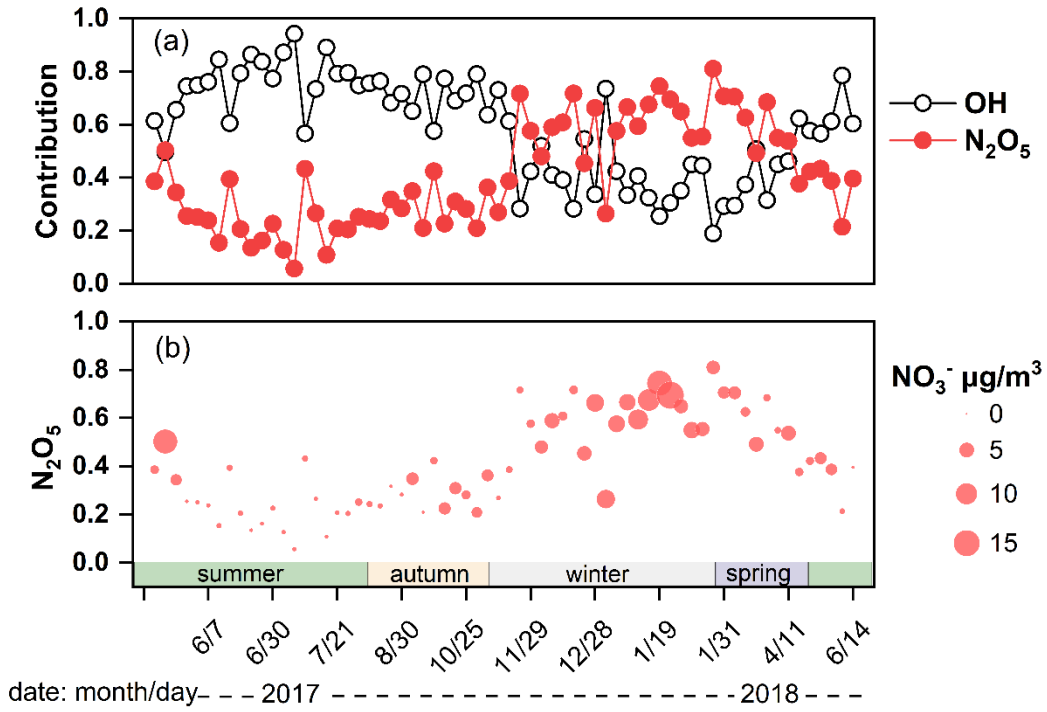

Figure 3. The contribution of the OH radical oxidation and N_2O_5 hydrolysis pathway to NO_3^- (a). The vertical position of dots corresponded to the contribution of N_2O_5 pathway and the size of the dots corresponded to the concentration of NO_3^- (b).

$\delta^{18}O\text{-}NO_3^-$ decreased from 76.7‰ in 2014 to 68.1‰ in 2017-2018(Zong et al., 2020), which indicated that ·OH channel became more important in Guangzhou. The enhanced contribution of ·OH pathway indicated the increasing atmospheric oxidation capacity. In recent years, although the concentration of $PM_{2.5}$ in Guangzhou has significantly decreased, the photochemical pollution caused by high O_3 concentrations was not optimistic(Tan et al., 2019). The O_3 concentration in the PRD showed a fluctuating upward trend from 2013 to 2020; especially in 2017-2018, O_3 concentrations were at high levels (Environmental Status Bulletin of Guangdong Province **Fig. S5**). In our study, the NO_3^- formation pathway inferred from $\delta^{18}O\text{-}NO_3^-$ proved the enhancement of atmospheric oxidation capacity.

3.3.2. Seasonal variation of $\delta^{15}N\text{-}NO_3^-$ and source apportionment of NO_3^-

Seasonal variation of $\delta^{15}N\text{-}NO_3^-$. The $\delta^{15}N\text{-}NO_3^-$ in Guangzhou was 4.9±2.2‰ (-0.4‰ to 10.8‰), which was similar to the wet deposition(Fang et al., 2011). The $\delta^{15}N\text{-}NO_3^-$ was comparable to that from the Northeast United States (6.8‰)(Elliott et al., 2009), and lower than regions in China, where NO_3^- was predominantly derived from anthropogenic sources, such as Heshan in Guangdong (7.50±3.30‰)(Su et al., 2020), Beihuangcheng Island (8.2±6.2‰)(Zong et al., 2017), and Beijing (12.1±3.3‰)(Fan et al., 2022). Nevertheless, the $\delta^{15}N\text{-}NO_3^-$ in this study was significantly higher than those from clean background regions, where NO_3^- was mainly from natural sources, such as the coast of Antarctica (-12.0±15.6‰)(Savarino et al., 2007) and Bermuda (-2.1±1.5‰ warm season, -5.9±3.3‰ cold season)(Hastings et al., 2003). The values of $\delta^{15}N\text{-}NO_3^-$ in winter, spring, summer, and autumn were 5.6‰, 5.3‰, 4.4‰, and 4.5‰, respectively. The $\delta^{15}N\text{-}NO_3^-$ in winter and summer showed significant difference ($p < 0.05$). The values of $\delta^{15}N\text{-}NO_3^-$ were influenced by atmospheric processes and emission sources(Elliott et al., 2009). For N_2O_5 channel, NO_3^- is characterized by higher $\delta^{15}N$ values(Freyer et al., 1993; Elliott et al., 2009). The N_2O_5 channel was the predominant formation pathway of NO_3^- in winter, which was in accordance with the seasonal variation in $\delta^{15}N\text{-}NO_3^-$. In addition, the difference in $\delta^{15}N\text{-}NO_3^-$ reflected the variation

in the emission source of NO_3^-. δ^{15}N-NOx from coal combustion was relatively high. In winter, the higher δ^{15}N-NO_3^- was probably related to long-range transport from North, where coal combustion enhanced in winter.

Source apportionment of NO_3^-. Based on the Bayesian mixing model coupled with δ^{15}N-NO_3^-, NO_3^- sources were assigned as coal combustion 40.4±8.7%, biomass burning 25.6±2.1%, mobile sources (vehicles) 22.3±3.1%, and microbial process 11.7±3.8%. **Figure 2b** and **Fig. S6** showed the source contribution of NO_3^- in Guangzhou and other regions in China, respectively. Compared to earlier periods (2013-2014), the concentration of NO_3^- from vehicle and coal combustion decreased significantly(Zong et al., 2020), which resulted from the stricter vehicle emission standard, promotion of new energy electric vehicles, and ultraclean transformation of coal combustion(Guangdongprovince, 2014; Tang et al., 2019). However, almost all production and domestic segments rely on energy generated from coal combustion, which was still dominant source of NO_3^- in 2017-2018. Coal combustion was affected not only by local emissions but also by external air mass transmission. The contribution of coal combustion was higher in winter than in summer, which probably related to the long-range transportation from the North. Taking 10 January 2018 as an example, the contribution of coal combustion sources to NO_3^- was 67.5%, and the corresponding air mass was from the North and transmitted to Guangzhou through high altitude. However, the air mass on 26 July 2017 was mainly from the South China Sea, which was transmitted through low-altitude to Guangzhou. The contribution of coal burning to NO_3^- on 26 July 2017 was 28.5% lower than that on 10 January 2018.

As non-fossil combustion source, biomass burning was also an important source of NO_3^- and accounted for 25.6%. The contribution of biomass burning and vehicle was stable throughout a year. Generally, high intensity biomass burning occurred in winter in Guangdong province (dry season, i.e., from November to March)(Xu et al., 2019). K^+ is a typical tracer of biomass burning. The concentration of K^+ enhanced in winter (0.4μg/m^3) was higher than that in summer (0.2μg/m^3) and autumn (0.2μg/m^3), respectively, indicating enhancement of biomass burning intensity. Also, NO_3^- concentration of biomass burning remarkably enhanced in winter (1.2μg/m^3), and was higher than that in summer (0.4μg/m^3) and autumn (0.3μg/m^3), respectively. However, coal combustion also enhanced in winter due to the demand for heating

in North China. Our sampling site was influenced by the air mass with high coal combustion contribution from the North by long-range transportation, which may reduce the contribution of biomass burning relatively. Thus, the contribution of biomass burning showed stable compared with coal combustion. Another non-fossil source is related to soil microbial activity and only contributed 11.7% to NO_3^-, which was unexpectedly lower than the results in earlier periods (2013-2014). Generally, the microorganisms in soil emit NO through nitrification or denitrification, which was affected by the amount of carbon and nitrogen nutrients in soil(Hall and Matson, 1996). In earlier periods, due to the higher level of aerosols, the amount of nutrients settling in soil was also higher, which was exemplified by the observation of dry and wet deposition in Guangzhou(He et al., 2022; Zheng et al., 2020). In addition, the reduction of cultivated land from 2013 to 2018 might also reduce the contribution of microbial source emissions. Therefore, emissions from natural sources were also influenced by human activities to some extent. The contribution of microbial process was higher in summer than in winter. In summer, higher RH and temperature were favorable for the intense activity of soil microorganisms(Zong et al., 2017). The contributions of microbial processes to NO_3^- also decreased in winter compared with summer at regional background sites and five Chinese megacities, including Guangzhou(Zong et al., 2017; Zong et al., 2020).

The sources comparison between NO_3^- and NH_4^+ was shown in **Fig. 2c**. Coal combustion, biomass burning, and vehicles were three significant sources of NO_3^- and NH_4^+. Coal combustion and biomass burning were the dominant sources of NO_3^- and NH_4^+, respectively. The vehicles were also an important source of atmospheric inorganic Nr contributed to 22.3% and 19.8% of NO_3^- and NH_4^+, respectively. Recently, the government has actively taken many measures to reduce the pollution from vehicles, such as stricter automobile emission standards and the promotion of new energy vehicles. However, due to the large vehicle ownership base, the pollutants emitted from vehicles are not optimistic. In addition, vehicles emissions could contribute half of the fresh secondary organic aerosol in urban environment(Zhang et al., 2022; Zhao et al., 2022a).

4. Conclusions

A year-long field observation was conducted in Guangzhou to clarify the atmospheric fate of inorganic nitrogen aerosol. Inorganic nitrogen species were the most essential component of TN including NH_4^+ (45.8%) and NO_3^- (23.2%), which are also dominant components of SIA and play a key role in China haze. The $\delta^{15}N$ is a powerful tool to quantify the source contribution of NH_4^+ and NO_3^-, which suggested that anthropogenic combustion sources (coal combustion, biomass burning, and vehicles) were the dominant sources.

Anthropogenic combustion sources contributed 63.2% to NH_4^+ higher than agricultural sources (23.6%). NH_3 largely facilitates the formation of sulfate and nitrate. Meanwhile, sulfate and nitrate promote each other with positive feedback effect, which could trigger haze. In megacities of China, the focus of NH_3 reduction should be on anthropogenic combustion sources, especially on biomass burning, which might be responsible for the lag of the decline in the deposition of air pollutions behind the reduction in emission(Zhao et al., 2022b). In addition, anthropogenic combustion sources accounted for 88.3% of NO_3^-. Coal combustion and vehicles contributed 40.4% and 22.3% to NO_3^-, respectively. Despite a series of measures to reduce emissions of NOx, fossil fuels, as the main energy for production and living, will still inevitably emit a large amount of NOx. Our results emphasized that the emission of atmospheric inorganic nitrogen is largely related to anthropogenic combustion sources. The development and promotion of clean energy and efficient use of biomass are conducive to the deep reduction of atmospheric nitrogen.

Data availability

The original data of this research (stable nitrogen isotopes and inorganic nitrogen concentrations) are available at Mendeley data (Li and Li, 2023). The Iso Source model was downloaded from Environmental Protection Agency, via their website: https://www.epa.gov/sites/default/files/2015-11/isosourcev1_3_1.zip.

Author contributions

Funding acquisition: Jun Li

Investigation: Tingting Li, Zeyu Sun, and Hongxing Jiang

Methodology: Tingting Li, Zeyu Sun, Hongxing Jiang, Jun Li, and Chongguo Tian

Project Administration: Jun Li

Resources: Jun Li, Chongguo Tian, and Gan Zhang

Software: Tingting Li, Zeyu Sun, and Chongguo Tian

Validation: Tingting Li and Jun Li

Writing – original draft: Tingting Li

Writing – review & editing: Jun Li

Competing interests

The authors declare that they have no conflict of interest.

Financial support

This study was supported by the Natural Science Foundation of China (NSFC; Nos. (41977177), Guangdong Basic and Applied Basic Research Foundation (2021A1515011456), Guangdong Foundation for Program of Science and Technology Research (Grant No. 2019B121205006 and 2020B1212060053).

References

Baskaran, M., K., B. S., and F., M. D.: Oxygen isotope dynamics of atmospheric nitrate and its precursor molecules. In Handbook of Environmental Isotope Geochemistry., Springer-Verlag Berlin Heidelberg2011.

Bhattarai, H., Zhang, Y. L., Pavuluri, C. M., Wan, X., Wu, G., Li, P., Cao, F., Zhang, W., Wang, Y., Kang, S., Ram, K., Kawamura, K., Ji, Z., Widory, D., and Cong, Z.: Nitrogen speciation and isotopic composition of aerosols collected at Himalayan Forest (3326 m a.s.l.): seasonality, sources, and implications, Environ. Sci. Technol., 53, 12247-12256, https://doi.org/10.1021/acs.est.9b03999, 2019.

Bhattarai, N., Wang, S., Pan, Y., Xu, Q., Zhang, Y., Chang, Y., and Fang, Y.: δ^{15}N-stable isotope analysis of NHx : An overview on analytical measurements, source sampling and its source apportionment, Front. Environ. Sci. Eng., 15, 126, https://doi.org/10.1007/s11783-021-1414-6, 2021.

Bhattarai, N., Wang, S., Xu, Q., Dong, Z., Chang, X., Jiang, Y., and Zheng, H.: Sources of gaseous NH_3 in urban Beijing from parallel sampling of NH_3 and NH_4^+, their nitrogen isotope measurement and modeling, Sci. Total Environ., 747, 141361, https://doi.org/10.1016/j.scitotenv.2020.141361, 2020.

Breemen, N. V.: Nitrogen cycle natural organic tendency, Nature, 415, https://doi.org/10.1038/415381a, 2002.

Chang, Y., Liu, X., Deng, C., Dore, A. J., and Zhuang, G.: Source apportionment of atmospheric ammonia before, during, and after the 2014 APEC summit in Beijing using stable nitrogen isotope signatures, Atmos. Chem.

Phys., 16, 11635-11647, https://doi.org/10.5194/acp-16-11635-2016, 2016.
Chen, Z., Pei, C., Liu, J., Zhang, X., Ding, P., Dang, L., Zong, Z., Jiang, F., Wu, L., Sun, X., Zhou, S., Zhang, Y., Zhang, Z., Zheng, J., Tian, C., Li, J., and Zhang, G.: Non-agricultural source dominates the ammonium aerosol in the largest city of South China based on the vertical $\delta^{15}N$ measurements, Sci. Total Environ., 848, 157750, https://doi.org/10.1016/j.scitotenv.2022.157750, 2022a.
Chen, Z. L., Song, W., Hu, C. C., Liu, X. J., Chen, G. Y., Walters, W. W., Michalski, G., Liu, C. Q., Fowler, D., and Liu, X. Y.: Significant contributions of combustion-related sources to ammonia emissions, Nat. Commun., 13, 7710, https://doi.org/10.1038/s41467-022-35381-4, 2022b.
Cui, M., Chen, Y., Zheng, M., Li, J., Tang, J., Han, Y., Song, D., Yan, C., Zhang, F., Tian, C., and Zhang, G.: Emissions and characteristics of particulate matter from rainforest burning in the Southeast Asia, Atmos. Environ., 191, 194-204, https://doi.org/10.1016/j.atmosenv.2018.07.062, 2018.
Dunne, E. M., Gordon, H., Kürten, A., Almeida, J., Duplissy, J., Williamson, C., Ortega, I. K., Pringle, K. J., Adamov, A., and Schobesberger, S.: Global atmospheric particle formation from cern cloud measurements, Science, 354, 1119-1123, https://doi.org/10.1126/science.aaf2649, 2016.
Elliott, E. M., Kendall, C., Wankel, S. D., Burns, D. A., Boyer, E. W., Harlin, K., Bain, D. J., and Butler, T. J.: Nitrogen isotopes as indicators of NOx source contributions to atmospheric nitrate deposition across the midwestern and Northeastern United States, Environ. Sci. Technol., 41, 7661-7667, https://doi.org/10.1021/es070898t, 2007.
Elliott, E. M., Kendall, C., Boyer, E. W., Burns, D. A., Lear, G. G., Golden, H. E., Harlin, K., Bytnerowicz, A., Butler, T. J., and Glatz, R.: Dual nitrate isotopes in dry deposition: Utility for partitioning NOx source contributions to landscape nitrogen deposition, J. Geophys. Res. , 114, https://doi.org/10.1029/2008JG000889, 2009.
Fan, M.-Y., Zhang, Y.-L., Hong, Y., Lin, Y.-C., Zhao, Z.-Y., Cao, F., Sun, Y., Guo, H., and Fu, P.: Vertical differences of nitrate sources in urban boundary layer based on tower measurements, Environ. Sci. Technol. Lett., 2c00600, https://doi.org/10.1021/acs.estlett.2c00600, 2022.
Fan, M. Y., Zhang, Y. L., Lin, Y. C., Cao, F., Zhao, Z. Y., Sun, Y., Qiu, Y., Fu, P., and Wang, Y.: Changes of emission sources to nitrate aerosols in Beijing after the clean air actions: evidence from dual isotope compositions, J. Geophys. Res.: Atmos., 125, 031998, https://doi.org/10.1029/2019jd031998, 2020.
Fang, Y. T., Koba, K., Wang, X. M., Wen, D. Z., Li, J., Takebayashi, Y., Liu, X. Y., and Yoh, M.: Anthropogenic imprints on nitrogen and oxygen isotopic composition of precipitation nitrate in a nitrogen-polluted city in southern China, Atmos. Chem. Phys., 11, 1313-1325, https://doi.org/10.5194/acp-11-1313-2011, 2011.
Felix, J. D. and Elliott, E. M.: The agricultural history of human-nitrogen interactions as recorded in ice core $\delta^{15}N$-NO_3^-, Geophys. Res. Lett., 40, 1642-1646, https://doi.org/10.1002/grl.50209, 2013.
Felix, J. D., Elliott, E. M., and Shaw, S. L.: Nitrogen isotopic composition of coal-fired power plant NOx: influence of emission controls and implications for global emission inventories, Environ. Sci. Technol., 46, 3528-3535, https://doi.org/10.1021/es203355v, 2012.
Felix, J. D., Elliott, E. M., Gish, T. J., McConnell, L. L., and Shaw, S. L.: Characterizing the isotopic composition of atmospheric ammonia emission sources using passive samplers and a combined oxidation-bacterial denitrifier approach, Rapid Commun. Mass Spectrom., 27, 2239-2246, https://doi.org/10.1002/rcm.6679, 2013.
Felix, J. D., Elliott, E. M., Avery, G. B., Kieber, R. J., Mead, R. N., Willey, J. D., and Mullaugh, K. M.: Isotopic composition of nitrate in sequential Hurricane Irene precipitation samples: Implications for changing NOx sources, Atmos. Environ., 106, 191-195, https://doi.org/10.1016/j.atmosenv.2015.01.075, 2015.
Fibiger, D. L. and Hastings, M. G.: First Measurements of the Nitrogen Isotopic Composition of NOx from

546 Biomass Burning, Environ. Sci. Technol., 50, 11569-11574, https://doi.org/10.1021/acs.est.6b03510, 2016.
547 Freyer, H. D., Kley, D., Volz-Thomas, A., and Kobel, K.: On the interaction of isotopic exchange processes with
548 photochemical reactions in atmospheric oxides of nitrogen, J. Geophys. Res. , 98, 14,791-714,796,
549 https://doi.org/10.1029/93JD00874, 1993.
550 Fu, X., Wang, S., Xing, J., Zhang, X., Wang, T., and Hao, J.: Increasing ammonia concentrations reduce the
551 effectiveness of particle pollution control achieved via SO_2 and NO_X emissions reduction in East China,
552 Environ. Sci. Technol. Lett., 4, 221-227, https://doi.org/10.1021/acs.estlett.7b00143, 2017.
553 Galloway, J. N., Dentener, F. J., Capone, D. G., Boyer, E. W., Howarth, R. W., Seitzinger, S. P., Asner, G. P.,
554 Cleveland, C. C., Green, P. A., Holland, E. A., Karl, D. M., Michaels, A. F., Porter, J. H., Townsend, A. R.,
555 and VörO¨smarty, C. J.: Nitrogen cycles past present and future, Biogeochemistry, 70, 153-226,
556 https://doi.org/10.1007/s10533-004-0370-0, 2004.
557 Gobel, A. R., Altieri, K. E., Peters, A. J., Hastings, M. G., and Sigman, D. M.: Insights into anthropogenic nitrogen
558 deposition to the North Atlantic investigated using the isotopic composition of aerosol and rainwater nitrate,
559 Geophys. Res. Lett., 40, 5977-5982, https://doi.org/10.1002/2013gl058167, 2013.
560 Action Plan for Air Pollution Control of Guangdong Province (2014-2017):
561 http://www.gd.gov.cn/gkmlpt/content/0/142/mpost_142687.html, last access: February 14, 2014.
562 Hall, S. J. and Matson, P. A.: NOx emissions from soil: implications for air quality modeling in agricultural regions,
563 Annu. Rev. Energy Environ., 21, 311-346, https://doi.org/10.1146/annurev.energy.21.1.311, 1996.
564 Hastings, M. G., Sigman, D. M., and Lipschultz, F.: Isotopic evidence for source changes of nitrate in rain at
565 Bermuda, J. Geophys. Res.: Atmos., 108, 1-12, https://doi.org/10.1029/2003jd003789, 2003.
566 He, S., Huang, M., Zheng, L., Chang, M., Chen, W., Xie, Q., and Wang, X.: Seasonal variation of transport
567 pathways and potential source areas at high inorganic nitrogen wet deposition sites in southern China, J.
568 Environ. Sci. (China), 114, 444-453, https://doi.org/10.1016/j.jes.2021.12.024, 2022.
569 Heaton, T. H. E., Spiro, B., and Robertson, S. M. C.: Potential canopy influences on the isotopic composition of
570 nitrogen and sulphur in atmospheric deposition, Oecologia, 109, 600-607, 1997.
571 Heeb, N. V., Forss, A.-M., Brühlmann, S., Lüscher, R., Saxer, C. J., and Hug, P.: Three-way catalyst-induced
572 formation of ammonia—velocity- and acceleration-dependent emission factors, Atmos. Environ., 40, 5986-
573 5997, https://doi.org/10.1016/j.atmosenv.2005.12.035, 2006.
574 Hodas, N., Sullivan, A. P., Skog, K., Keutsch, F. N., Collett, J. L., Jr., Decesari, S., Facchini, M. C., Carlton, A.
575 G., Laaksonen, A., and Turpin, B. J.: Aerosol liquid water driven by anthropogenic nitrate: implications for
576 lifetimes of water-soluble organic gases and potential for secondary organic aerosol formation, Environ. Sci.
577 Technol., 48, 11127-11136, https://doi.org/10.1021/es5025096, 2014.
578 Holland, E. A., Dentener, F. J., Braswell, B. H., and Sulzman, J. M.: Contemporary and pre-industrial global
579 reactive nitrogen budgets, Biogeochemistry, 46, 7-43, https://doi.org/10.1007/BF01007572, 1999.
580 Huang, S., Elliott, E. M., Felix, J. D., Pan, Y., Liu, D., Li, S., Li, Z., Zhu, F., Zhang, N., Fu, P., and Fang, Y.:
581 Seasonal pattern of ammonium ^{15}N natural abundance in precipitation at a rural forested site and implications
582 for NH_3 source partitioning, Environ. Pollut., 247, 541-549, https://doi.org/10.1016/j.envpol.2019.01.023,
583 2019.
584 Huang, Z., Wang, S., Zheng, J., Yuan, Z., Ye, S., and Kang, D.: Modeling inorganic nitrogen deposition in
585 Guangdong province, China, Atmos. Environ., 109, 147-160,
586 https://doi.org/10.1016/j.atmosenv.2015.03.014, 2015.
587 Jiang, H., Li, J., Sun, R., Tian, C., Tang, J., Jiang, B., Liao, Y., Chen, C., and Zhang, G.: Molecular dynamics and
588 light absorption properties of atmospheric dissolved organic matter, Environ. Sci. Technol., 55, 10268-10279,
589 https://doi.org/10.1021/acs.est.1c01770, 2021a.

Jiang, H., Li, J., Sun, R., Liu, G., Tian, C., Tang, J., Cheng, Z., Zhu, S., Zhong, G., Ding, X., and Zhang, G.: Determining the sources and transport of brown carbon using radionuclide tracers and modeling, J. Geophys. Res.: Atmos., 126, e2021JD034616, https://doi.org/10.1029/2021jd034616, 2021b.

Johnston, J. C. and Thiemens, M. H.: The isotopic composition of tropospheric ozone in three environments, J. Geophys. Res.: Atmos., 102, 25395-25404, https://doi.org/10.1029/97jd02075, 1997.

Kang, Y., Liu, M., Song, Y., Huang, X., Yao, H., Cai, X., Zhang, H., Kang, L., Liu, X., Yan, X., He, H., Zhang, Q., Shao, M., and Zhu, T.: High-resolution ammonia emissions inventories in China from 1980 to 2012, Atmos. Chem. Phys., 16, 2043-2058, https://doi.org/10.5194/acp-16-2043-2016, 2016.

Kawashima, H. and Kurahashi, T.: Inorganic ion and nitrogen isotopic compositions of atmospheric aerosols at Yurihonjo, Japan: implications for nitrogen sources, Atmos. Environ., 45, 6309-6316, https://doi.org/10.1016/j.atmosenv.2011.08.057, 2011.

Kundu, S., Kawamura, K., and Lee, M.: Seasonal variation of the concentrations of nitrogenous species and their nitrogen isotopic ratios in aerosols at Gosan, Jeju Island: Implications for atmospheric processing and source changes of aerosols, J. Geophys. Res. , 115, https://doi.org/10.1029/2009jd013323, 2010.

Li, T. and Li, J.: High contribution of anthropogenic combustion sources to atmospheric inorganic reactive nitrogen in south China evidenced by isotopes, Mendeley data [data set], https://doi.org/10.17632/yck5xy22w2.1, 2023.

Li, X. H. and Wang, S. X.: Particulate and trace gas emissions from open burning of wheat straw and corn stover in China, Environ. Sci. Technol., 41, 6052-6058, https://doi.org/10.1021/es0705137, 2007.

Liao, B., Wu, D., Chang, Y., Lin, Y., Wang, S., and Li, F.: Characteristics of particulate SO_4^{2-}, NO_3^-, NH_4^+, and related gaseous pollutants in Guangzhou (in Chinese), Acta Sci. Circumst., 34, 1551-1559, https://doi.org/10.13671/j.hjkxxb.2014.0218, 2014.

Liu, J., Ding, P., Zong, Z., Li, J., Tian, C., Chen, W., Chang, M., Salazar, G., Shen, C., Cheng, Z., Chen, Y., Wang, X., Szidat, S., and Zhang, G.: Evidence of rural and suburban sources of urban haze formation in China: a case study from the Pearl River Delta region, J. Geophys. Res.: Atmos., 123, 4712-4726, https://doi.org/10.1029/2017jd027952, 2018.

Liu, T., Wang, X., Wang, B., Ding, X., Deng, W., Lü, S., and Zhang, Y.: Emission factor of ammonia (NH_3) from on-road vehicles in China: tunnel tests in urban Guangzhou, Environ. Res. Lett., 9, 064027, https://doi.org/10.1088/1748-9326/9/6/064027, 2014.

Liu, Y., Zhang, Y., Lian, C., Yan, C., Wang, Y., Ge, M., He, H., and Kulmala, M.: The promotion effect of nitrous acid on aerosol formation in wintertime in Beijing: the possible contribution of traffic-related emissions, Atmos. Chem. Phys., 20, 13023–13040, https://doi.org/10.5194/acp-20-13023-2020, 2020.

Liu, Y., Feng, Z., Zheng, F., Bao, X., Liu, P., Ge, Y., Zhao, Y., Jiang, T., Liao, Y., Zhang, Y., Fan, X., Yan, C., Chu, B., Wang, Y., Du, W., Cai, J., Bianchi, F., Petäjä, T., Mu, Y., He, H., and Kulmala, M.: Ammonium nitrate promotes sulfate formation through uptake kinetic regime, Atmos. Chem. Phys., 21, 13269–13286, https://doi.org/10.5194/acp-21-13269-2021, 2021.

Martinellia, L. A., Camargoa, P. B., Laraa, L. B. L. S., Victoriaa, R. L., and Artaxo, P.: Stable carbon and nitrogen isotopic composition of bulk aerosol particles in a C4 plant landscape of southeast Brazil, Atmos. Environ., 36, 2427–2432, https://doi.org/10.1016/S1352-2310(01)00454-X, 2002.

Meng, W., Zhong, Q., Yun, X., Zhu, X., Huang, T., Shen, H., Chen, Y., Chen, H., Zhou, F., Liu, J., Wang, X., Zeng, E. Y., and Tao, S.: Improvement of a global high-resolution ammonia emission inventory for combustion and industrial sources with new data from the residential and transportation sectors, Environ. Sci. Technol., 51, 2821-2829, https://doi.org/10.1021/acs.est.6b03694, 2017.

Meng, Z., Xu, X., Lin, W., Ge, B., Xie, Y., Song, B., Jia, S., Zhang, R., Peng, W., Wang, Y., Cheng, H., Yang, W.,

and Zhao, H.: Role of ambient ammonia in particulate ammonium formation at a rural site in the North China Plain, Atmos. Chem. Phys., 18, 167-184, https://doi.org/10.5194/acp-18-167-2018, 2018.

Michalski, G., Bhattacharya, S. K., and Girsch, G.: NOx cycle and the tropospheric ozone isotope anomaly: an experimental investigation, Atmos. Chem. Phys., 14, 4935-4953, https://doi.org/10.5194/acp-14-4935-2014, 2014.

Pan, Y., Tian, S., Liu, D., Fang, Y., Zhu, X., Gao, M., Gao, J., Michalski, G., and Wang, Y.: Isotopic evidence for enhanced fossil fuel sources of aerosol ammonium in the urban atmosphere, Environ. Pollut., 238, 942-947, https://doi.org/10.1016/j.envpol.2018.03.038, 2018a.

Pan, Y., Tian, S., Liu, D., Fang, Y., Zhu, X., Zhang, Q., Zheng, B., Michalski, G., and Wang, Y.: Fossil fuel combustion-related emissions dominate atmospheric ammonia sources during severe haze episodes: evidence from ^{15}N-stable isotope in size-resolved aerosol ammonium, Environ. Sci. Technol., 50, 8049-8056, https://doi.org/10.1021/acs.est.6b00634, 2016.

Pan, Y., Tian, S., Liu, D., Fang, Y., Zhu, X., Gao, M., Wentworth, G. R., Michalski, G., Huang, X., and Wang, Y.: Source Apportionment of Aerosol Ammonium in an Ammonia-Rich Atmosphere: An Isotopic Study of Summer Clean and Hazy Days in Urban Beijing, J. Geophys. Res.: Atmos., 123, 5681-5689, https://doi.org/10.1029/2017jd028095, 2018b.

Pan, Y., Gu, M., He, Y., Wu, D., Liu, C., Song, L., Tian, S., Lü, X., Sun, Y., Song, T., Walters, W. W., Liu, X., Martin, N. A., Zhang, Q., Fang, Y., Ferracci, V., and Wang, Y.: Revisiting the concentration observations and source apportionment of atmospheric ammonia, Adv. Atmos. Sci., 37, 933-938, https://doi.org/10.1007/s00376-020-2111-2, 2020.

Qu, K., Wang, X., Xiao, T., Shen, J., Lin, T., Chen, D., He, L. Y., Huang, X. F., Zeng, L., Lu, K., Ou, Y., and Zhang, Y.: Cross-regional transport of $PM_{2.5}$ nitrate in the Pearl River Delta, China: Contributions and mechanisms, Sci. Total Environ., 753, 142439, https://doi.org/10.1016/j.scitotenv.2020.142439, 2021.

Savarino, J., Kaiser, J., Morin, S., Sigman, D. M., and Thiemens, M. H.: Nitrogen and oxygen isotopic constraints on the origin of atmospheric nitrate in coastal Antarctica, Atmos. Chem. Phys., 7, 1925–1945, https://doi.org/10.5194/acp-7-1925-2007, 2007.

Song, W., Liu, X. Y., Hu, C. C., Chen, G. Y., Liu, X. J., Walters, W. W., Michalski, G., and Liu, C. Q.: Important contributions of non-fossil fuel nitrogen oxides emissions, Nat. Commun., 12, 243, https://doi.org/10.1038/s41467-020-20356-0, 2021.

Song, Y., Dai, W., Wang, X., Cui, M., Su, H., Xie, S., and Zhang, Y.: Identifying dominant sources of respirable suspended particulates in Guangzhou, China, Environ. Eng. Sci., 25, 959-968, https://doi.org/10.1089/ees.2007.0146, 2008.

Su, T., Li, J., Tian, C., Zong, Z., Chen, D., and Zhang, G.: Source and formation of fine particulate nitrate in South China: Constrained by isotopic modeling and online trace gas analysis, Atmos. Environ., 231, https://doi.org/10.1016/j.atmosenv.2020.117563, 2020.

Sun, X., Zong, Z., Li, Q., Shi, X., Wang, K., Lu, L., Li, B., Qi, H., and Tian, C.: Assessing the emission sources and reduction potential of atmospheric ammonia at an urban site in Northeast China, Environ. Res., 198, 111230, https://doi.org/10.1016/j.envres.2021.111230, 2021.

Tan, Z., Lu, K., Jiang, M., Su, R., Wang, H., Lou, S., Fu, Q., Zhai, C., Tan, Q., Yue, D., Chen, D., Wang, Z., Xie, S., Zeng, L., and Zhang, Y.: Daytime atmospheric oxidation capacity in four Chinese megacities during the photochemically polluted season: a case study based on box model simulation, Atmos. Chem. Phys., 19, 3493–3513, https://doi.org/10.5194/acp-19-3493-2019, 2019.

Tang, L., Qu, J., Mi, Z., Bo, X., Chang, X., Anadon, L. D., Wang, S., Xue, X., Li, S., Wang, X., and Zhao, X.: Substantial emission reductions from Chinese power plants after the introduction of ultra-low emissions

678 standards, Nat. Energy, 4, 929-938, https://doi.org/10.1038/s41560-019-0468-1, 2019.
679 Urey, H. C.: The thermodynamic properties of isotopic substances, J. Chem. Soc., 562-581,
680 https://doi.org/10.1039/jr9470000562, 1947.
681 Walters, W. W. and Michalski, G.: Theoretical calculation of oxygen equilibrium isotope fractionation factors
682 involving various NOy molecules, OH, and H_2O and its implications for isotope variations in atmospheric
683 nitrate, Geochim. Cosmochim. Ac., 191, 89–101 https://doi.org/10.1016/j.gca.2016.06.039, 2016.
684 Walters, W. W., Simonini, D. S., and Michalski, G.: Nitrogen isotope exchange between NO and NO_2 and its
685 implications for $\delta^{15}N$ variations in tropospheric NOx and atmospheric nitrate, Geophys. Res. Lett., 43, 440-
686 448, https://doi.org/10.1002/2015gl066438, 2016.
687 Walters, W. W., Tharp, B. D., Fang, H., Kozak, B. J., and Michalski, G.: Nitrogen Isotope Composition of
688 Thermally Produced NOx from Various Fossil-Fuel Combustion Sources, Environ. Sci. Technol., 49, 11363-
689 11371, https://doi.org/10.1021/acs.est.5b02769, 2015.
690 Walters, W. W., Song, L., Chai, J., Fang, Y., Colombi, N., and Hastings, M. G.: Characterizing the spatiotemporal
691 nitrogen stable isotopic composition of ammonia in vehicle plumes, Atmos. Chem. Phys., 20, 11551-11567,
692 https://doi.org/10.5194/acp-20-11551-2020, 2020.
693 Wang, C., Duan, J., Ren, C., Liu, H., Reis, S., Xu, J., and Gu, B.: Ammonia emissions from croplands decrease
694 with farm size in China, Environ. Sci. Technol., 56, 9915-9923, https://doi.org/10.1021/acs.est.2c01061,
695 2022.
696 Wang, T., Xue, L., Brimblecombe, P., Lam, Y. F., Li, L., and Zhang, L.: Ozone pollution in China: a review of
697 concentrations, meteorological influences, chemical precursors, and effects, Sci. Total Environ., 575, 1582-
698 1596, https://doi.org/10.1016/j.scitotenv.2016.10.081, 2017.
699 Wang, X., Carmichael, G., Chen, D., Tang, Y., and Wang, T.: Impacts of different emission sources on air quality
700 during March 2001 in the Pearl River Delta (PRD) region, Atmos. Environ., 39, 5227-5241,
701 https://doi.org/10.1016/j.atmosenv.2005.04.035, 2005.
702 Wang, X., Wu, Z., Shao, M., Fang, Y., Zhang, L., Chen, F., Chan, P.-w., Fan, Q., Wang, Q., Zhu, S., and Bao, R.:
703 Atmospheric nitrogen deposition to forest and estuary environments in the Pearl River Delta region, southern
704 China, Tellus B: Chem. Phys. Meteorol., 65, https://doi.org/10.3402/tellusb.v65i0.20480, 2013.
705 Wedin, D. A. and Tilman, D.: Influence of nitrogen loading and species composition on the carbon balance of
706 grasslands, Science, 274, https://doi.org/10.1126/science.274.5293.1720, 1996.
707 Wu, L., Ren, H., Wang, P., Chen, J., Fang, Y., Hu, W., Ren, L., Deng, J., Song, Y., Li, J., Sun, Y., Wang, Z., Liu,
708 C.-Q., Ying, Q., and Fu, P.: Aerosol ammonium in the urban boundary layer in Beijing: insights from nitrogen
709 isotope ratios and simulations in summer 2015, Environ. Sci. Technol. Lett., 6, 389-395,
710 https://doi.org/10.1021/acs.estlett.9b00328, 2019.
711 Xiang, Y.-K., Dao, X., Gao, M., Lin, Y.-C., Cao, F., Yang, X.-Y., and Zhang, Y.-L.: Nitrogen isotope characteristics
712 and source apportionment of atmospheric ammonium in urban cities during a haze event in Northern China
713 Plain, Atmos. Environ., 269, 118800, https://doi.org/10.1016/j.atmosenv.2021.118800, 2022.
714 Xiao, H. W., Wu, J. F., Luo, L., Liu, C., Xie, Y. J., and Xiao, H. Y.: Enhanced biomass burning as a source of
715 aerosol ammonium over cities in central China in autumn, Environ. Pollut., 266, 115278,
716 https://doi.org/10.1016/j.envpol.2020.115278, 2020.
717 Xu, Y., Huang, Z., Jia, G., Fan, M., Cheng, L., Chen, L., Shao, M., and Zheng, J.: Regional discrepancies in
718 spatiotemporal variations and driving forces of open crop residue burning emissions in China, Sci. Total
719 Environ., 671, 536-547, https://doi.org/10.1016/j.scitotenv.2019.03.199, 2019.
720 Yang, Y., Li, P., He, H., Zhao, X., Datta, A., Ma, W., Zhang, Y., Liu, X., Han, W., Wilson, M. C., and Fang, J.:
721 Long-term changes in soil pH across major forest ecosystems in China, Geophys. Res. Lett., 42, 933-940,

https://doi.org/10.1002/2014gl062575, 2015.
Yu, X., Shen, L., Hou, X., Yuan, L., Pan, Y., An, J., and Yan, S.: High-resolution anthropogenic ammonia emission inventory for the Yangtze River Delta, China, Chemosphere, 251, 126342, https://doi.org/10.1016/j.chemosphere.2020.126342, 2020.
Zhang, Z., Zeng, Y., Zheng, N., Luo, L., Xiao, H., and Xiao, H.: Fossil fuel-related emissions were the major source of NH_3 pollution in urban cities of northern China in the autumn of 2017, Environ. Pollut., 256, 113428, https://doi.org/10.1016/j.envpol.2019.113428, 2020.
Zhang, Z., Zhu, W., Hu, M., Wang, H., Tang, L., Hu, S., Shen, R., Yu, Y., Song, K., Tan, R., Chen, Z., Chen, S., Canonaco, F., Prevot, A. S. H., and Guo, S.: Secondary organic aerosol formation in China from urban-lifestyle sources: Vehicle exhaust and cooking emission, Sci. Total Environ., 857, 159340, https://doi.org/10.1016/j.scitotenv.2022.159340, 2022.
Zhao, Y., Tkacik, D. S., May, A. A., Donahue, N. M., and Robinson, A. L.: Mobile sources are still an important source of secondary organic aerosol and fine particulate matter in the los angeles region, Environ. Sci. Technol., 56, 15328-15336, https://doi.org/10.1021/acs.est.2c03317, 2022a.
Zhao, Y., Xi, M., Zhang, Q., Dong, Z., Ma, M., Zhou, K., Xu, W., Xing, J., Zheng, B., Wen, Z., Liu, X., Nielsen, C. P., Liu, Y., Pan, Y., and Zhang, L.: Decline in bulk deposition of air pollutants in China lags behind reductions in emissions, Nat. Geosci., 15, 190-195, https://doi.org/10.1038/s41561-022-00899-1, 2022b.
Zheng, L., Chen, W., Jia, S., Wu, L., Zhong, B., Liao, W., Chang, M., Wang, W., and Wang, X.: Temporal and spatial patterns of nitrogen wet deposition in different weather types in the Pearl River Delta (PRD), China, Sci. Total Environ., 740, 139936, https://doi.org/10.1016/j.scitotenv.2020.139936, 2020.
Zhu, J., He, N., Wang, Q., Yuan, G., Wen, D., Yu, G., and Jia, Y.: The composition, spatial patterns, and influencing factors of atmospheric wet nitrogen deposition in Chinese terrestrial ecosystems, Sci. Total Environ., 511, 777-785, https://doi.org/10.1016/j.scitotenv.2014.12.038, 2015.
Zong, Z., Shi, X., Sun, Z., Tian, C., Li, J., Fang, Y., Gao, H., and Zhang, G.: Nitrogen isotopic composition of NOx from residential biomass burning and coal combustion in North China, Environ. Pollut., 304, 119238, https://doi.org/10.1016/j.envpol.2022.119238, 2022.
Zong, Z., Tan, Y., Wang, X., Tian, C., Li, J., Fang, Y., Chen, Y., Cui, S., and Zhang, G.: Dual-modelling-based source apportionment of NOx in five Chinese megacities: providing the isotopic footprint from 2013 to 2014, Environ. Int., 137, 105592, https://doi.org/10.1016/j.envint.2020.105592, 2020.
Zong, Z., Wang, X., Tian, C., Chen, Y., Fang, Y., Zhang, F., Li, C., Sun, J., Li, J., and Zhang, G.: First assessment of NOx sources at a regional background site in North China using isotopic analysis linked with modeling, Environ. Sci. Technol., 51, 5923-5931, https://doi.org/10.1021/acs.est.6b06316, 2017.